Loss Analysis and Performance Improvement of Very Low Specific Speed Centrifugal Pumps

Shusaku KAGAWA* Yokohama National Univ., Japan d06sb103@ynu.ac.jp
Jun MATSUI Yokohama National Univ., Japan jmat@ynu.ac.jp
Junichi KUROKAWA Yokohama National Univ., Japan kuro@post.me.ynu.ac.jp
Young-Do CHOI Yokohama National Univ., Japan ydchoi@mach.me.ynu.ac.jp

Key words: Turbomachinary, Centrifugal Pump, Very Low Specific Speed, CFD, Loss Analysis, Performance Improvement

Abstract

In the range of very low specific speed n_s, improvement of efficiency is the most important subject in order to apply turbo machine to such a low specific speed range. The purpose of the present study is focused on the performance improvement of pump in the range of $n_s \leq 80[m, m^3/min, min^{-1}]$, and CFD simulation is performed to determine the reason why efficiency is very low. Moreover, in order to obtain very low specific speed impeller with high efficiency, a new type centrifugal impeller with radial grooves mounted at the back of both front and rear shrouds is simulated and tested to reveal the performance improvement.

The result shows that a rapidly increase of leakage rate and disk friction rate with a decrease of n_s is the main reason of low efficiency. Also, the result shows that if the leakage loss is reduced by use of Labyrinth seal at $n_s = 25$, the disk friction rapidly increases in spite of the leakage reduction and pump overall efficiency becomes only 5% higher. Moreover, the new type impeller with grooves produces very high-head compared with that of normal impeller at $n_s = 80$.

Introduction

Efficiency of a centrifugal pump drops rapidly with a decrease of specific speed n_s(Ref 1). In the very low n_s range, such as $n_s \leq 80[m, m^3/min, min^{-1}]$, efficiency of a centrifugal pump becomes low and positive-displacement pump has long been used. However, because of vibration and noise problems of positive-displacement pump, the application of a centrifugal pump to such a low n_s range is strongly required.

As for the performance characteristics of a centrifugal pump, many studies have long been conducted and the optimum design method is established for the range of normal specific speed ($n_s \geq 100$). But, little is known about the performance characteristics of a very low n_s pump, as there are few studies, and it is difficult to attain high efficiency by conventional design methods.

One of the present authors studied pump performance of $n_s = 80$ and determined the effects of design parameters on pump performance (Ref 2). But, in the range of $n_s \leq 60$, the spiral

angle γ of a volute casing becomes very small and a circular casing is suitable for a pump casing.

It is well known that best efficiency point (BEP) of a centrifugal pump is determined as the intersection point of both impeller head curve and casing head curve (Ref 3). In the very low n_s range, the BEP is mainly determined by a casing head curve, and the cross-sectional area of casing tongue influences mainly on the casing head curve. It is also revealed that the maximum efficiency of a pump specially designed for a very low n_s is lower than the efficiency of a rather higher n_s pump operated at partial load. After all, a very low n_s pump can only be realized by reducing the sectional area of a volute tongue, and an improvement of efficiency can be attained by using a circular casing and by operating a higher n_s pump at partial load (Ref 4). In order to further improve the pump efficiency, it is necessary to reveal the loss mechanism and to reduce the main loss in the very low n_s range.

One of serious problems in the low n_s pump is an unstable head-capacity curves. Near the shut-off point the head curves tend to have rising characteristics (Ref 2). One of the present authors clarified that radial vanes attached at the back of impeller shroud increases pumping head by about 20%, and improved unstable head curves (Ref 5). Instead of radial vanes, shallow radial grooves (J-Groove (Ref 6)) are expected to have almost same effect as radial vanes.

The present study is intended to improve performance of very low n_s pump, and loss mechanism is analyzed by CFD, and a new device is proposed to improve pump performance.

Numerical Analysis and Experimental Apparatus

Test centrifugal pumps for CFD

In order to reveal the loss mechanism of a very low n_s pump, centrifugal pumps of n_s = 114, 80, 60, 40 and 25 are adopted (Ref 2) (Ref 4) (Ref 5). The dimensions of the simulated centrifugal pumps are shown in Table 1. Every impeller is closed type and the impeller outlet angle β_2 is 60°.

To be remarked in Table 1 is the following 2 points; One is that the impeller outlet width b_2 is selected relatively large. This is because the conventional design gives too small impeller outlet width to manufacture (Ref 1) (Ref 7), the limit of which is $b_2/r_2 \leq 0.02$, and because relatively large b_2 results in better efficiency (Ref 2). The other is that a seal clearance is comparatively large in the very low n_s range. This is because the large seal clearance result is a higher efficiency due to the reduction of disk friction (Ref 8) in case of n_s = 80 and 60 (Ref 2).

To realize the pumps of n_s = 25 and 40, the same casing and impeller are used but the sectional area of volute tongue is different (Ref 4). In the low n_s range, $n_s \leq 60$, a circular casing is used. The test Reynolds number based on u_2 is $Re = u_2 r_2/\nu = 2.7 \sim 3.2 \times 10^6$.

Table 1 Dimensions of test pumps simulated

n_s	β_2 [°]	r_2 [mm]	b_2 [mm]	Z	Casing type	Seal type (Clearance)	γ [°]
114	60	135	8	8	Spiral	Labyrinth (0.1mm)	1.1
80	60	101	2.5	6	Spiral	Wearing ring (3.5mm)	0.9
60	60	129	5.2	6	Circular	Wearing ring (5mm)	0
40	60	126	6.3	6	Circular	Wearing rong (5mm)	0
25	60	126	6.3	6	Circular	Wearing ring (5mm)	0

Numerical analysis

Numerical analysis is conducted using commercial CFD code ANSYS CFX (Ref 9). All the CFD simulation is performed by unsteady simulation using Reynolds Averaged Navier-Stokes equation and $k-\omega$ turbulence model. Applied boundary conditions are uniform velocity at the inlet and average static pressure at the outlet, respectively. Figure 1 shows the calculation grid of a centrifugal pump of n_s = 80 and the number of computational grid is about 1.2 millions in every case. The gap flow at the back of impeller is also calculated as shown in Fig.1 (c). Eight grids are placed at the seal clearance, and it is confirmed that the leakage flow rate ϕ_q and disk friction torque τ_{disk} is almost same when the grids are increased to 16. All interfaces, for example inlet to impeller and leakage outlet interface, are set to Transient Rotor-Stator interface.

At each calculation at first a steady-state calculation is carried out and the result is used to initialize the unsteady calculation. The time step of the unsteady calculation has been set to 6.25×10^{-4} seconds, and the calculations are carried out for half impeller revolutions in n_s = 25 cases. It is also confirmed that time-averaged head and torque are almost same when total time has been changed to one impeller revolutions at any discharge in n_s = 60 cases. And in the n_s = 25 case, CPU-time of unsteady calculation in one discharge required about 3 times longer than that of steady-state calculations.

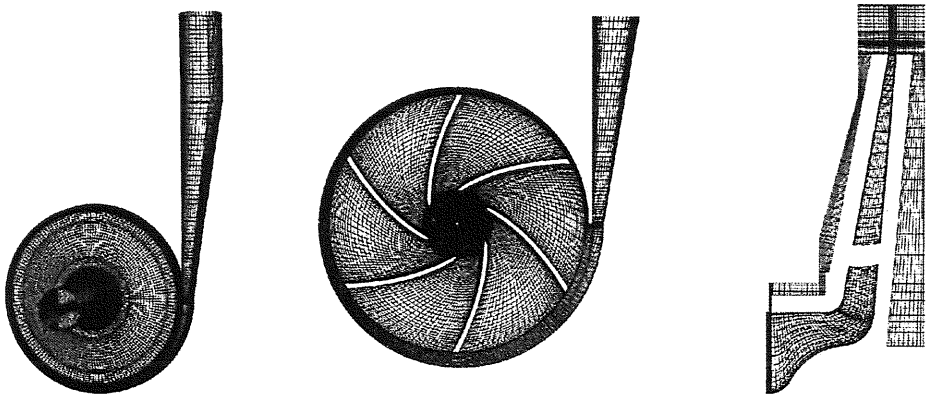

(a) Outside view **(b) Front view** **(c) Side view**

Figure 1 Computational grid of centrifugal pump at specific speed 80

Analysis of pump shaft power and efficiency

In order to clarify the cause of low efficiency, pump shaft power and efficiency are analyzed. The pump shaft power of a closed impeller is expressed as follows.

$$\tau = \left(\phi_Q + \phi_q\right)\psi_{th} + \tau_{disk} + \tau_R \tag{1}$$

Theoretical head coefficient ψ_{th} is composed of actual head coefficient ψ and non-dimensional hydraulic loss $h_{loss} = \Delta H/(u_2^2/2g)$ in an impeller channel, a parallel-walled diffuser and a volute casing. Thus Eq.(1) becomes as follows.

$$\tau = \phi_Q\left(\psi + h_{imp.} + h_{diffuser} + h_{casing}\right) + \phi_q\psi_{th} + \tau_{disk} + \tau_R \tag{2}$$

where $\phi_Q\psi$ shows the pump output, $\phi_Q h_{imp.}$ the power loss due to impeller channel hydraulic loss, $\phi_Q h_{diffuser}$ the power loss due to parallel wall-diffuser hydraulic loss, $\phi_Q h_{casing}$ the power loss due to casing hydraulic loss, $\phi_q\psi_{th}$ the power loss due to leakage, τ_{disk} the disk friction

power, and τ_R the loss power due to inlet reverse flow, respectively. Hydraulic loss can be calculated by the difference of mass-flow averaged total pressure at each position. τ_R is estimated by angular momentum change at the impeller inlet section.

New type impeller with J-Groove and Experimental apparatus

The above loss analysis revealed that both the disk friction loss and leakage loss are relatively large in the range of $n_s \leq 60$ compared with those of ordinary specific speed centrifugal pump. Since the disk friction is proportional to the fifth power of radius r_2, it is important to reduce the impeller outlet radius. Thus, if pumping head is increased by J-Groove, performance improvement based on reducing the impeller outlet radius is possible.

In order to clarify the effect of J-Groove, CFD simulation was also performed before experiment. For the reason above, the geometry of J-Groove is different from CFD and experiment. Dimensions and configurations of the tested and simulated J-Grooves are shown in Fig. 2 and Table 2. Computational grid of simulated J-Groove is also shown in Fig.2 (b). Though the J-Groove has many dimensional parameters, their effects are known to be represented by a single parameter "JE No." defined as follows (Ref 6);

$$JENo. = (n_G W/2\pi)^{1/5} (DW)(2D + W)(L/2W)^{1/2}$$

where $D = d/r_2$, $W = w/r_2$ and $L = l/r_2$. JE No. of each groove is also shown in Table 2.

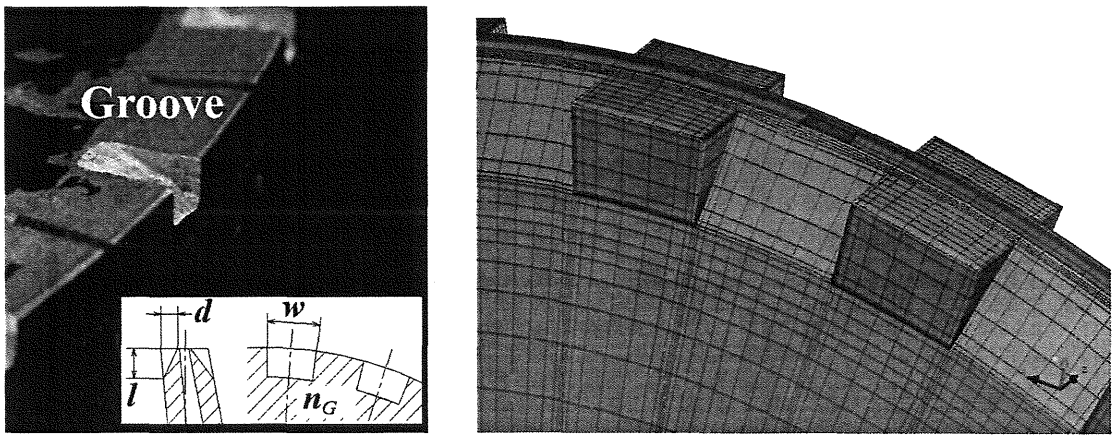

(a) Test groove **(b) Grid formation in groove**

Figure 2 Photograph and Grid of J-Groove at specific speed 80

Table 2 Dimensions of J-Groove

Gr No.	location	w [mm]	d [mm]	l [mm]	JE No. [$\times 10^{-5}$]
Normal		0	0	0	0
A	front & rear	1	4	10	8.1
B	front & rear	5	4	10	36.2
C	front & rear	10	4	10	81.4
D	front	10	4	10	40.7
CFD	front & rear	13.2	4.5	8	123.0

Results and Discussions

Comparison of CFD results with experimental results

Comparisons of the CFD results with experiments of pump performances of all simulated centrifugal pumps are shown in Fig. 3. Figure 3 reveals that all the CFD results are in good agreement with the experimental data in all n_s ranges. Also, CFD results give good prediction to the unstable characteristics of head curve near the shut-off point. Though not shown in figures, pressure distribution around the impeller is also in good agreement with that of experiment.

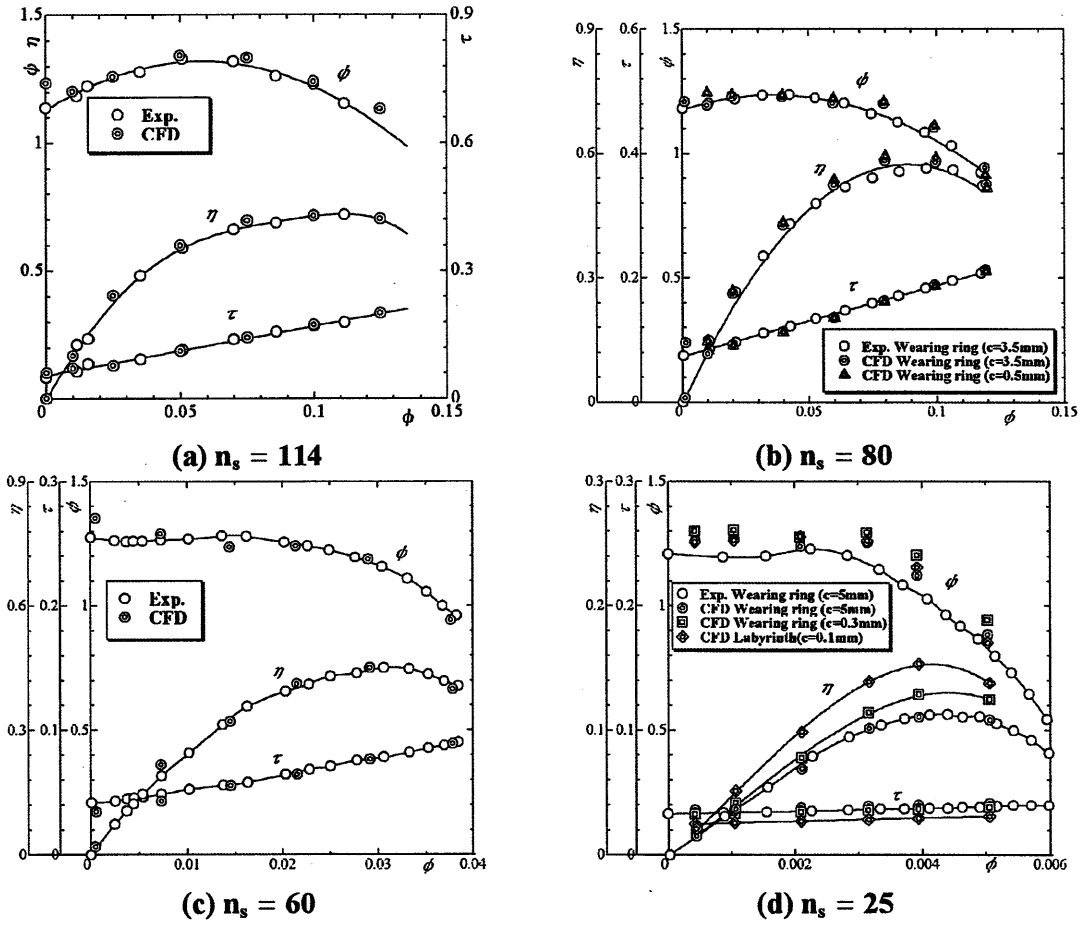

Figure 3 Comparison of performance curves of CFD simulation with Experiment

Loss analysis

Figure 4 (a) shows the CFD results of 3 kinds of efficiencies ; the hydraulic efficiency η_h, the mechanical efficiency η_m and the volumetric efficiency η_v at the BEP of all simulated centrifugal pumps, together with the disk friction ratio τ_{disk}/τ as a reference value. It is clearly revealed that volumetric efficiency drops largely with a decrease of specific speed. This is because pump discharge decreases with a decrease of specific speed, and the influence of leakage becomes relatively large. Mechanical efficiency also decreases, but the amount of drop is not so large. On the other hands, hydraulic efficiency rapidly decrease in the range of $n_s \leq 40$.

Figure 4 (b) shows CFD result of shaft power at BEP of all simulated centrifugal pumps, and each loss power calculated from Eq. (2). Figure 4 (b) clearly reveals the leakage loss and disk friction loss increases considerably with the decrease of n_s, and that the effective parameters on performance improvement in the range of $n_s \leq 60$ are power loss due to leakage and disk

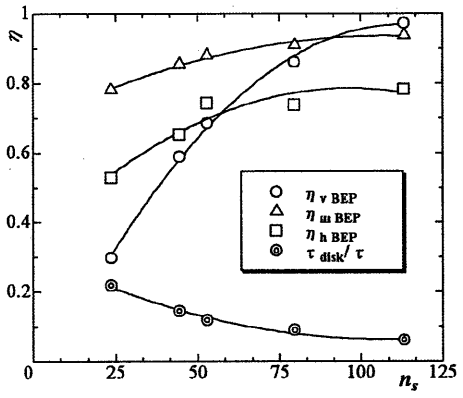

(a) Analysis of pump efficiency

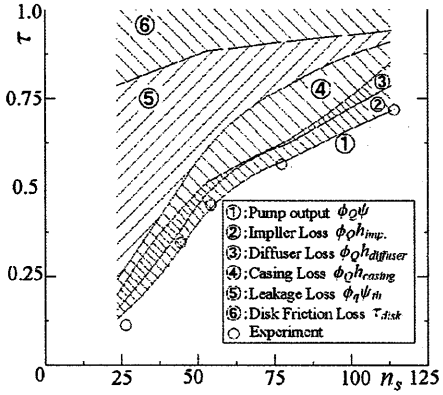

(b) Analysis of shaft power

Figure 4 Analysis of efficiency and shaft power at BEP (CFD)

friction. In addition, power loss due to impeller inlet reverse flow τ_R was also calculated, but influence of τ_R on shaft power was almost 3% at maximum. It is then concluded that power loss due to inlet reverse flow τ_R is not very large because impeller radius ratio r_1/r_2 is very small in a very low n_s impeller.

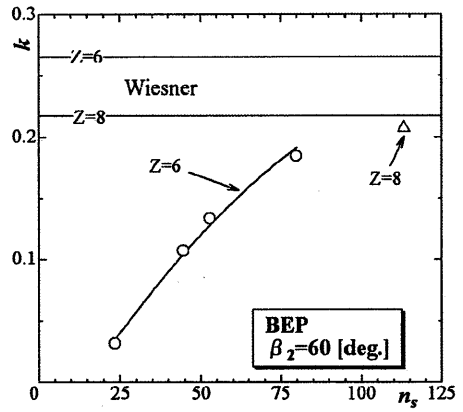

(a) Slip factor of all specific speed pump

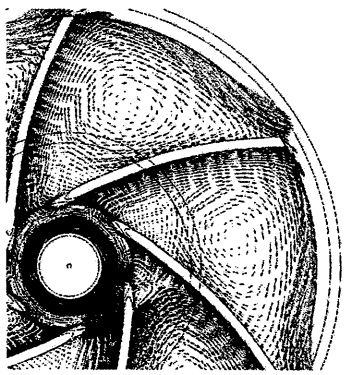

(b) Velocity vector at specific speed 25

Figure 5 Analysis of Pump Internal Flow (CFD)

Figure 4 (a) shows that η_h is very small in the very low n_s range, which implies that the theoretical head ψ_{th} becomes extraordinary large. In order to reveal the reason, slip factor is calculated and compared with Wiesner formula (Ref 10) in Fig. 5(a). Wiesner formula is known to give good prediction in the normal n_s range. Figure 5(a) reveals that the slip factor comes near to zero (no slip) with a decrease of n_s. This suggests that the impeller outlet flow pattern is near the ideal flow pattern of closed impeller. However, the calculated flow pattern shown in Fig. 5(b) reveals that large recirculation flow exists in every passage and it is much different from ideal flow pattern. This large recirculation flow once flows out from the impeller channel and flows into impeller again. This recirculating flow makes the mass flow averaged tangential velocity $\overline{\overline{V_{u2}}}$ very large. As a result, the theoretical head, defined as $\psi_{th} = 2\overline{\overline{V_{u2}}}/u_2$ becomes very large and hydraulic efficiency rapidly decreases. Therefore, improvement of impeller outlet flow might be inevitable in efficiency improvement of the very low n_s impellers.

Figure 4 also reveals that the reduction of leakage is of key importance for efficiency improvement in the very low n_s range. To reduce leakage, the calculation was further performed

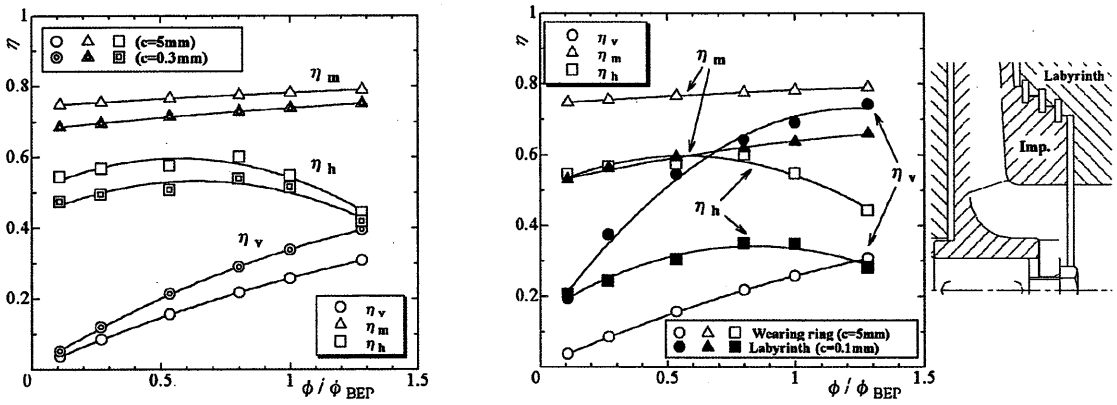

(a) Influence of seal clearance (c=5 and 0.3mm)

(b) Minimum clearance case by Labyrinth seal

Figure 6 Influence of seal clearance at n_s = 25 on efficiency (CFD)

by reducing the seal gap to 0.3 or 0.5 mm, and the results are compared in Fig.3 (b) for n_s = 80 and Fig.3(d) for n_s = 25. It is recognized that the reduction of seal gap does not improve overall efficiency in n_s = 80 and improves only 2% in n_s = 25. To reveal the reason why the efficiency rise is so small, each component of efficiencies is compared in Fig. 6 (a). Figure 6 (a) reveals that both η_m and η_h decrease to cancel the increase of η_v.

However, the loss analysis shown in Fig. 4 (b) reveals that 75% of all loss is occupied by the leakage loss, and the reduction of leakage should results in efficiency improvement if the seal clearance is reduced to the minimum attainable value. The Labyrinth seal is thus designed as shown at the right of Fig. 6 (b) to reduce the seal clearance to 0.1mm, and the component efficiencies are compared in Fig. 6 (b). It is clearly shown that η_v is improves considerably by 40% at the BEP, but η_h and η_m drops considerably. As a result the maximum efficiency rises by only 5% as shown in Fig.3 (d).

As mentioned above, the reduction of leakage is always accompanied with the increase of both disk friction torque and hydraulic loss in impeller channel in the very low n_s range.

Effect of J-Groove on pump performance

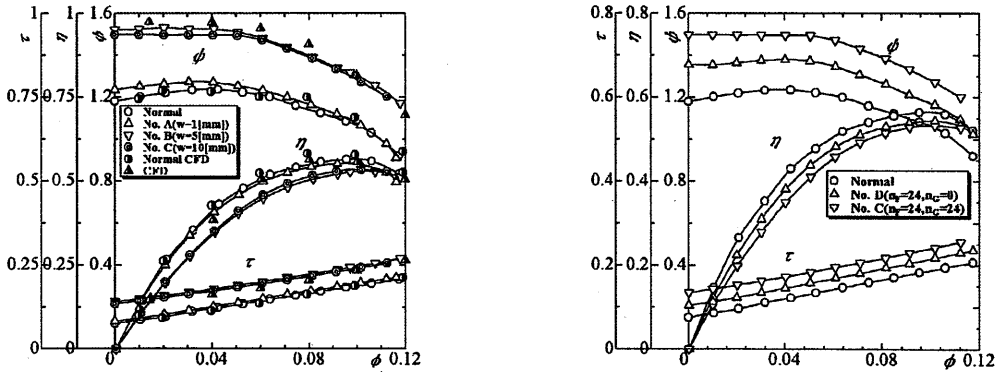

(a) Effect of J-Groove width

(b) J-Groove on one side and both case

Figure 7 Effect of J-Groove on pump performance (n_s = 80)

If pumping head is increased by J-Groove, performance improvement based on reducing the impeller outlet radius is expected. Figure 7 (a) shows the effect of J-Groove width on pump

performance curves. The dimensions of J-Groove are n_G = 24, d = 4[mm], l = 10[mm] and the width w is changed from 1 to 10mm. From Figure 7 (a) it is recognized that the head coefficient increases by about 30% (head rise of about 15[m]) by J-Groove. Shaft power also increases in parallel, and the maximum efficiency drops by about 3%. In addition, the unstable head-capacity curve near the shut-off point is much improved. Pump performance curves by CFD are also compared in Fig. 7 (a) and are in good prediction with experimental data in spite of J-Groove geometry differences. It is shown to be able to clarify the effect of J-Groove by CFD.

Figure 7 (b) shows the comparison of pump performance curves when J-Groove is mounted on one side and both sides. The effect of J-Groove mounted on both front and rear sides of impeller shroud improves to two times compare with the case of grooves on one side. Another J-Groove parameter, such as length, is also varied. However, effect of J-Groove length on pump performance is small compared with that of J-Groove width. As a conclusion, J-Groove mounted on both sides of impeller shroud is very effective and J-Groove width is the main influencing parameter on the pump performance. These results suggests that r_2 can be reduced to 88% ($H \propto r_2^2 \Rightarrow 1/\sqrt{1.3}$) by J-Groove under the same head.

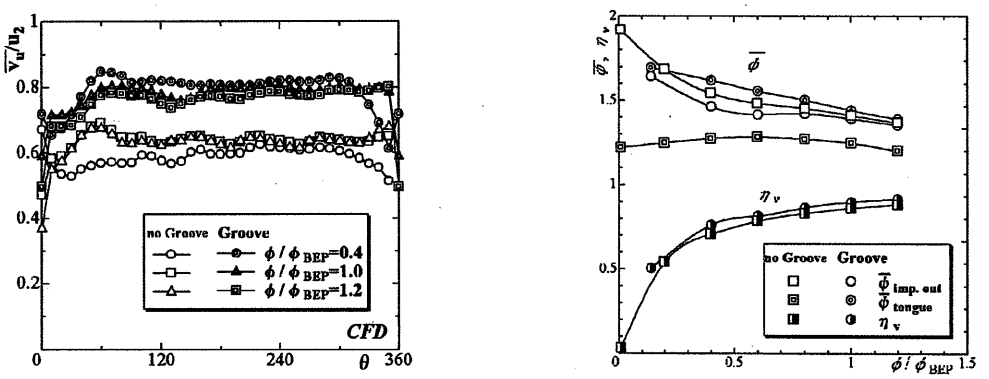

(a) Absolute tangential velocity along basic circle **(b) Total head at impeller outlet and casing tongue**

Figure 8 Performance improvement by J-groove (n_s = 80)

In order to reveal the reason why J-Groove makes pumping head so higher, the distribution of sectional average tangential velocity $\overline{v_u}/u_2$ around impeller (r/r_2 = 1.03) is calculated by CFD as shown in Fig. 8 (a). Figure 8 (b) shows the comparisons of mass flow-averaged total pressure at impeller outlet ($\overline{\overline{\psi_{imp.out}}}$) and at the casing outlet (casing tongue $\overline{\overline{\psi_{tongue}}}$) by CFD. Figure 8(a) reveals that tangential velocity $\overline{v_u}/u_2$ increases in parallel by adopting J-Groove. Though not shown in figures, pressure distribution around impeller was almost same as no groove case. As a result, the head rise by J-Groove is caused by the increase of dynamic pressure by fluid velocity.

Figure 8 (b) reveals that the head loss ($\overline{\overline{\psi_{imp.out}}} - \overline{\overline{\psi_{tongue}}}$) between impeller outlet and volute outlet is very large when J-Groove is not installed. On the other hands, when J-Groove is mounted on the impeller outlet, total pressure at the casing tongue becomes higher than that at the impeller outlet. This shows that J-Groove is working effectively to the fluid. As a conclusion, J-Groove reduces mixing loss between impeller outlet flow and volute flow and increases tangential velocity at impeller outlet. In addition, volumetric efficiency η_v changes little by the adoption of J-Groove.

It is concluded that head-rise and stable head curve are caused by J-Groove mounted at the back of both front and rear shrouds. In order to apply J-Groove to actual design, optimization of J-Groove configuration is necessary. Though there are many parameters in J-Groove configura-

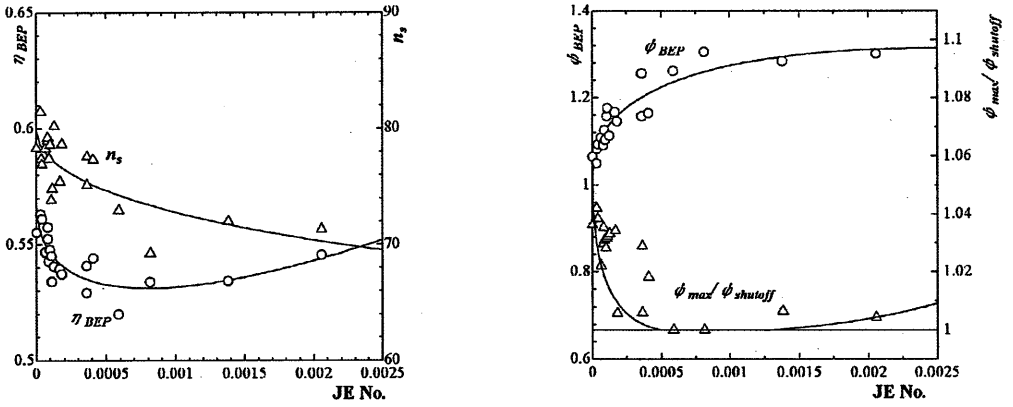

(a) η_{BEP} and n_s vs. JE No. **(b) ψ_{BEP} and $\psi_{max}/\psi_{shutoff}$ vs. JE No.**

Figure 9 Optimum Groove design chart (n_s = 80)

tion, the effect of J-Groove is represented by a single parameter, JE No.. Efficiency and specific speed at the BEP are shown against JE No. in Fig. 9 (a). Head coefficient at BEP and the ratio of maximum head to shut-off head are also shown against JE No. in Fig. 9 (b). If $\psi_{max}/\psi_{shut-off}$ value is 1.0, the head curve becomes stable. Both figures reveals that effectiveness of J-Groove has a limit, even though the effect of J-groove on pump performance is very large, and that the optimum J-Groove configuration is located in the range of JE No. $= 5.0 \times 10^{-4} \sim 1.2 \times 10^{-3}$ from the viewpoint of stable head curve.

Conclusions

In order to improve pump performance at $n_s \leq 80$, loss analysis by CFD is performed and a new type impeller with J-Groove is proposed and tested. The results are summarized as follows.

1. Power loss due to leakage and disk friction increases rapidly with the decrease of n_s in the very low n_s range. Especially, 75% of power loss is occupied by leakage loss at $n_s = 25$. However, if the leakage loss is reduced drastically, the disk friction loss and hydraulic loss in impeller channel increases considerably, and only 5% of efficiency rise is attained at $n_s = 25$.

2. The hydraulic efficiency at best efficiency point is almost constant in the range of $n_s = 60 \sim 80$. However, it drops rapidly in the range of $n_s \leq 40$.

3. An impeller with J-Groove is suitable in the range of very low specific speed. J-Groove rises pumping head by 30%, which is caused by rapid increase of dynamic pressure by fluid velocity in a volute. In addition, the unstable head-capacity curve becomes stable. These are suggested that performance improvement based on reduction of the impeller outlet radius is possible.

Acknowledgment

The authors express their sincere gratitude to Mr. M.Okazaki for his support in the performance measurements.

Reference

Ref 1 STEPANOFF, A. J., "Centrifugal and Axial Flow Pumps, 2nd ed.", John Wiley and Sons, 1957.

Ref 2 KUROKAWA, J., MATSUMOTO, K., MATSUI, J. and KITAHORA, T., "Performances of Centrifugal Pumps of Very Low Specific Speed", Proceedings 19th IAHR Sympo. on Hydraulic Machinery and Cavitaion, Singapore, 1998.

Ref 3 WORSTER, R. C., "The Flow in Volutes and its Effect on Centrifugal Pump Performance", Proceedings Inst. Mech. Eng, Vol. 177-31, pp.843-875., 1963.

Ref 4 KAGAWA, S., KUROKAWA, J., MATSUI, J., and CHOI, Y., "Performance of Very Low Specific Speed Centrifugal Pumps", Proceedings The 6th KSME-JSME Thermal and Fluids Engineering Conf., Jeju Korea, 2005.

Ref 5 KUROKAWA, J., YAMADA, T. and HIRAGA, H., "Performances of Low Specific Speed Centrifugal Pumps", Proceedings of 11th Austarlasian Fluid Mechnics Conf., Tasumania Australia, 1992.

Ref 6 SAHA,S L., KUROKAWA, J., MATSUI, J. and IMAMURA, H., "Suppression of Performance Curves Instability of a Mixed Flow Pump by Use of J-groove", Trans. ASME, Journal of Fluids Engineering, Vol.122-9, pp.592-597, 2000.

Ref 7 PFLEIDERER, C., "Die Kreiselpumpen für Flüssigkeiten und Gase 5 Aufl.", Springer- Verlag, 1961.

Ref 8 KUROKAWA, J. and Toyokura, T. "Axial Thrust, Disk Friction Torque and Leakage Loss of Radial Flow Turbomachinary", Proceedings of Pumps and Turbines Conf., Glasgow England, 1976.

Ref 9 ANSYS Inc., "ANSYS CFX Documentation Ver. 5.7.1", Waterloo, Ontario, Canada, 2004.

Ref 10 Wiesner,F.J, "A Review of Slip Factors for Centrifugal Impellers", Trans. ASME, Journal of Engineering for Power, Vol. 89-4, pp.558-572., 1967.

Nomenclature

b	:	channel width [mm]
d	:	depth of J-Groove [mm]
l	:	length of J-Groove [mm]
n_s	:	specific speed (= $n\sqrt{Q}/H^{3/4}$, n: revolution [$m, m^3/min, min^{-1}$])
n_G	:	number of J-Groove
r	:	radius [mm]
u_2	:	impeller tip speed [m/s]
v_u	:	absolute tangential velocity [m/s]
w	:	width of J-Groove [mm]
Z	:	number of impeller's blades
β_2	:	impeller outlet angle [deg.]
η	:	pump efficiency
θ	:	angle measured from casing tongue [deg.]
ϕ	:	discharge coefficient (= $Q/2\pi r_2 b_2 u_2$, Q: discharge)
ψ	:	head coefficient (= $2gH/u_2^2$, H: pumping head)
τ	:	shaft power coefficient (= $P/\pi\rho r_2 b_2 u_2^3$, P, ρ: shaft power, density, respectively)
Subscripts		
2,3	:	at impeller outlet, at volute basic circle, respectively
Q, q, th	:	pump discharge, leakage, theoretical, respectively
$\overline{\overline{A}}$	:	mass-flow averaged value of A
$\overline{A}$	:	sectional area averaged value of A